Simulation of a Bimetallic Alloy Cooling Process

R. Rozsnyo[1], A. Masserey[1], F. Carrard[1], V. Sanchez Mejia[1]
N. Hofmann[2], S. Maas[2], M. Hotic[2], P. Schoass[2]
H. Freisse[3], F. Lienard[3]

[1]hepia, HES-SO Geneva, University of Applied Sciences and Arts Western Switzerland
[2]FHNW, University of Applied Sciences and Arts Northwestern Switzerland
[3]Kugler Bimetal SA, Geneva, Switzerland

Abstract

In this paper we present a 3D Comsol Multiphysics simulation model of a bimetallic Tokat-steel alloy cooling process. The model is using the Turbulent Fluid Flow interface of the CFD module, the Heat Transfer in Fluids and Solids interface of the Heat-Transfer module and the Thermal-Structure interaction interface of the Structural Mechanics module. The phase change in the Tokat and the thermal radiation are considered. The residual stresses are computed with an elastoplastic material model. The level of shrinkage is estimated by the implementation of the Niyama criterion. The simulations allow to track the solid fraction and the solidification front, and to understand the cooling fluid flow distribution around the cooled part. The simulation results with Comsol Multiphysics are compared with experimental measurements of the temperature evolution at some points of the system.

Keywords: Forced Cooling, Niyama Criterion, Shrinkage, Residual Stresses, Multiphysics Simulation

Introduction

Kugler Bimetal is a company producing parts where Tokat, a tin-bronze material with lead (CuSn alloy), is cast onto a friction surface. The amount of lead may vary from less than 1 % to 30 %, depending on the specific application and thus covering a wild field of mechanical properties. Bimetallic mechanical parts made of steel and Tokat combine in an optimal manner the mechanical properties of the steel and the excellent anti-friction characteristics of the Tokat. These properties make applications possible in various high-tech domains such as aviation, energy and transports industries. In such components, one or more surfaces of the steel are covered with a thin layer of Tokat. The Tokat-steel interface features a zone of intermetallic diffusion of between 3 and 5 microns. This ensures perfect adhesion and, in every case the mechanical properties of the interface are superior to those of bronze itself. Steel and Tokat are linked in an inseparable fashion to form one part (Fig. 1). In the Kugler Bimetal process, the parts are produced by a process of gravity casting of Tokat onto steel. After casting, a major phase of the production is the cooling. After casting and cooling, the parts are re-machined. The way of cooling is fundamental to get a Tokat-steel interface with controlled shrinkage and without cracks. In the standard production process cooling rings and tubes are used to pulse air on the part to be cooled (Fig. 2). The temperature, the orientation and the velocity of the air flow influence the evolution of the solidification front in the Tokat. An imperfectly applied forced cooling will lead to a high level of shrinkage and cracks near the Tokat-steel interface. The cooling process is usually well known for parts with standard geometries. However, there is an increasing demand from the industry for parts with complex shapes. In such a case the optimisation of the cooling process may not be easy. Numerical investigations become necessary and are commonly used for such problems ([1], [2]).

Figure 1. An example of screw pumps manufactured by Kugler Bimetal

We explain in the following how we modelled the industrial process of cooling of a specific part with Comsol Multiphysics to predict shrinkage and residual stresses. The cooling system having no symmetries like most of the parts to be cooled, the geometry must be 3D. A full model coupling fluid

flow and heat transfer is possible. However, it has huge computation time cost. Thus, we followed an intermediate approach based on two observations:
a. while the cooling is forced, the conductive heat flow on the boundaries of the part to be cooled depends mainly on the fluid flow properties ([3]),
b. the fluid flow around the part is quasi stationary.
The idea was to compute an equivalent heat transfer coefficient on the boundaries of the part that may be used for heat transfer investigations allowing to understand the final state of the cooled component. Validation experiments were setup and the comparisons with the simulation results are presented. For the sake of confidentiality, we don't give the values of all the physical parameters that were used.

The Kugler Bimetal Industrial Process

The solid Tokat is placed in the hollowed part of the cylinder-shaped steel and covered with another steel plate on top of the crucible. The system is placed in a furnace to be heated to 1020 °C. When this temperature is reached, the Tokat is liquid but the steel remains solid. The system is removed from the furnace and placed in a cooling station. A thermal isolation strip is added on the upper limits of the steel crucible. The system, surrounded by an air domain, is then cooled by two cooling rings and a central tube (Fig. 2 & 3). The cooling has 2 phases:
Phase 1, the part is cooled by natural convection during 120 seconds after being removed from the furnace. This corresponds to the time necessary to bring the part from the oven to the cooling station. The environment is rather warm. The ambient temperature was measured to be $T_{amb} = 35$ °C.
Phase 2, the forced cooling is activated after 120 seconds and runs for 1'080 seconds. The total process (natural cooling + forced cooling) ends after 20 minutes.
At high temperatures, the part is red and yellow, the energy outflow at the boundaries of the part is dominated by radiation (Fig. 2).

Figure 2. The industrial process

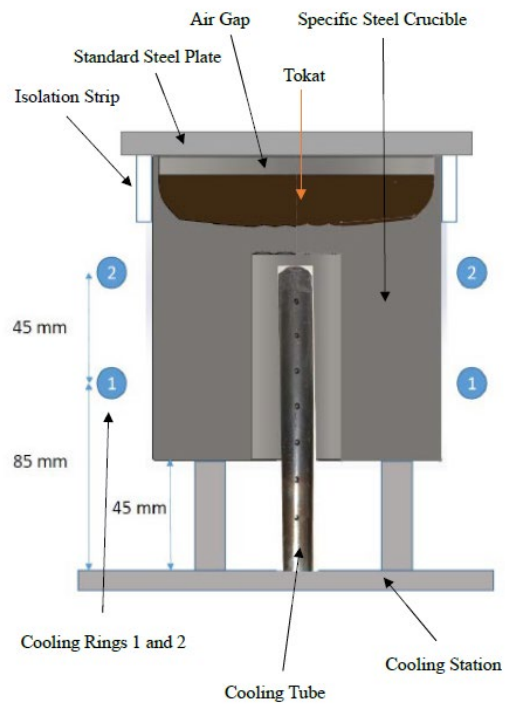

Figure 3. Schematic cross section of the part and the cooling system

Temperature Measurements

The temperature evolution was measured at some points during the cooling process. The component was positioned as centrally as possible in the cooling station. The volume flow was controlled by valves and the pressure in the cooling rings 1 and 2 (Fig. 3) was recorded.

Measurement on the component surface

Four holes with a depth of 6 mm were drilled for the measurement of the temperature on the surface of the component. Four thermocouples (Fig. 4) of type K were inserted manually in the holes after the component was removed from the furnace.

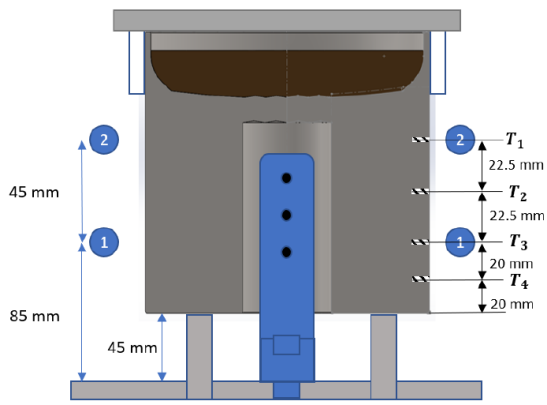

Figure 4. Lateral boundary thermocouples position

Measurement in the center of the part

Two holes with depth of 50 mm and 70 mm were drilled for the temperature measurement inside the component (Fig. 5).

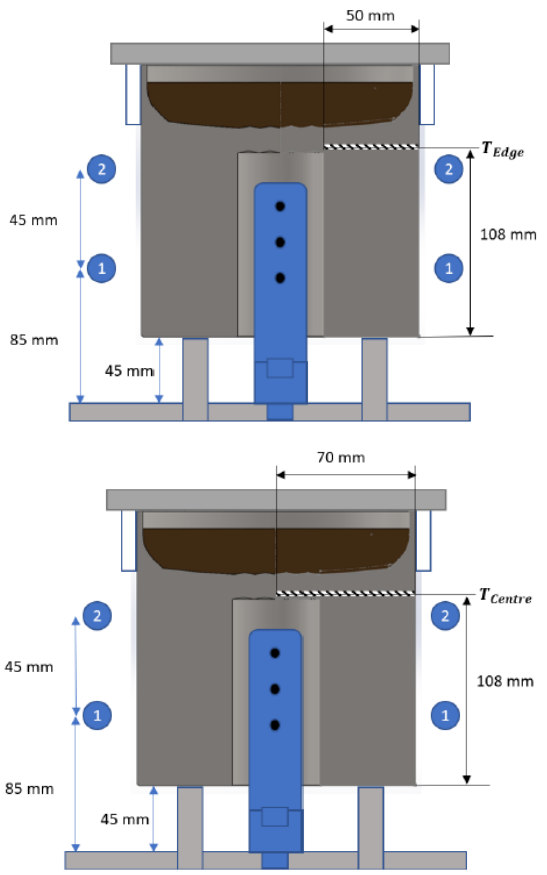

Figure 5. Internal thermocouples position

Type K coated thermocouples were already positioned in the holes before the component was heated up and thus heated up in the furnace.

Measurement of the Heat Transfer Coefficient

Measurements of the temperature were made by thermal camera. The temperature was inverse calculated by an algorithm to give the heat transfer coefficient at the surface. The Figure 6 shows the measured temperature distribution on the surface and the impact of the cooling rings.

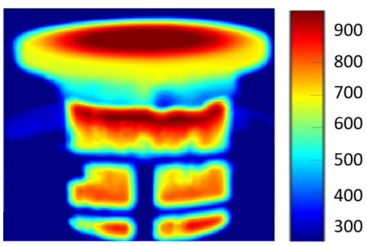

Figure 6. Temperature distribution in °C given by the thermal camera at t = 120 s.

Governing Equations

Fluid flow modelling

Due to the high injection average velocities leading to high Reynolds numbers, the air flow around the system is turbulent and incompressible. The gravity is considered, however, close to the part, due to the cooling rings and to the cooling tube, the natural convection may be neglected. Thus, to model the mean flow characteristics, the equations governing the flow are the standard turbulent k-ε Navier-Stokes equations. The momentum conservation is given by Eq. 1:

$$\rho_a \frac{\partial \boldsymbol{u}}{\partial t} + \rho_a (\boldsymbol{u} \cdot \nabla)\boldsymbol{u} = -\nabla \cdot (p\boldsymbol{I} + \boldsymbol{K}) + \rho_a \boldsymbol{g}, \quad (1)$$

where, $\boldsymbol{u}$ is the velocity field, $\boldsymbol{g}$ the gravity field, ρ_a the air density, p the pressure scalar field, $\boldsymbol{I}$ the identity tensor and $\boldsymbol{K}$ the viscous stress tensor. We have:

$$\boldsymbol{K} = (\mu_a + \mu_T)(\nabla \boldsymbol{u} + \nabla \boldsymbol{u}^T), \quad (2)$$

where μ_a is the air dynamic viscosity and μ_T is the turbulent viscosity calculated thanks to the variables k and ε, solutions of additional equations ([4]). We must add to Eq. 1 the equation of the mass conservation:

$$\nabla \cdot \boldsymbol{u} = 0. \quad (3)$$

Eq. 1 and Eq. 3 must be completed by the boundary and the initial conditions. The boundary conditions are on the exterior boundaries of the fluid domain an « Open Boundary » condition and a « Slip » wall boundary condition on the parts boundaries and on the ground. The injection holes of the rings and the tube have an « Inlet » boundary condition with a prescribed normal injection velocity for each hole. The velocities are ramped with a smooth step function over 10 seconds to avoid numerical instabilities. At the initial time, corresponding to the time $t = 120\ s$, the air is assumed to have a velocity field $\boldsymbol{u} = \boldsymbol{0}$. The pressure field is given by the relation corresponding to the fundamental law of the hydrostatics:

$$p = p_{ref} + \rho_a \boldsymbol{g} \cdot (\boldsymbol{r} - \boldsymbol{r}_{ref}). \quad (4)$$

Heat transfer in solids and fluids modelling

The heat transfer in all media may be described by Eq. 5:

$$\rho C_p \frac{\partial T}{\partial t} + \rho C_p \boldsymbol{u} \cdot \nabla T - \nabla \cdot (-k \nabla T) = 0, \quad (5)$$

where, ρ is the density of a given material, C_p its heat capacity at constant pressure and k its thermal conductivity. In the solid domains the velocity field must be taken to be $\boldsymbol{u} = \boldsymbol{0}$. We have a coupling between Eq. 1 and Eq. 5 in the air surrounding the system to be cooled through the Boussinesq approximation on the air density:

$$\rho_a = \rho_{ref}(1 - \alpha_p)(T - T_{ref}), \tag{6}$$

where ρ_{ref} is the reference density of the air, i.e. at the reference temperature, $T_{ref} = 20$ °C, and α_p is the dilatation coefficient at constant pressure at the reference temperature given by:

$$\alpha_p = -\frac{1}{\rho_a}\left(\frac{\partial \rho_a}{\partial T}\right)_p. \tag{7}$$

In the Tokat, where phase change occurs, the density, the heat capacity and the heat conductivity were calculated by the Thermo-Calc software in function of the temperature, covering the phase change range of temperatures. We deduced the value of the latent heat used in the phase change model, between the solidus (690 °C) and the liquidus (987 °C) temperatures, thanks to the solid fraction curve given in function of the temperature by the Figure 6.

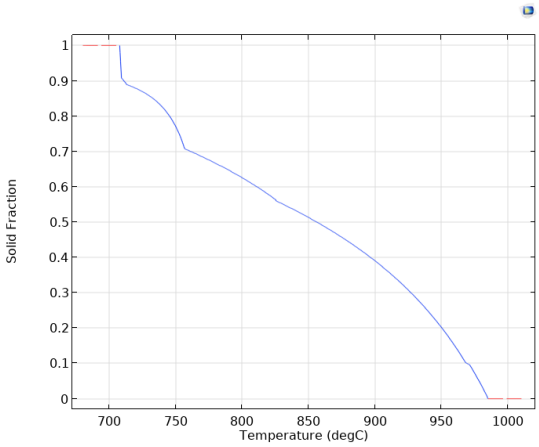

Figure 6. Solid fraction in function of the temperature

Eq. 5 must be completed by boundary and initial conditions. The computational domain doesn't include the cooling rings and the cooling tube. Their boundaries are set to « Thermal Insulation » when there is no forced cooling. While forced cooling occurs, the boundaries corresponding to the injection holes are set to a constant temperature, the temperature of the pulsed air, that is T_{amb}. An exterior infinite element layer was added to the air domain to simulate an unbounded environment (Fig.7). The boundary condition on these exterior boundaries is also the constant temperature T_{amb}. A thin thermal resistive layer was added to the steel boundary to model the thermal effect of the oxidation layer. The process having two phases, the initial conditions for the second phase are given by the last state of the system in the phase one.

Thermomechanics modelling

Under cooling in their solid state, the Tokat and the crucible steel are submitted to thermal expansion. In our case the expansion is negative which means contraction. We must couple the heat transfer equations with the general equation of structural mechanics:

$$\rho \frac{\partial^2 \boldsymbol{u}}{\partial t^2} = \nabla \cdot (\boldsymbol{F}\boldsymbol{S})^{\mathrm{T}} + \boldsymbol{F}_v, \tag{8}$$

where, $\boldsymbol{u}$ is the displacement field, $\boldsymbol{F}_v$ the density of volume forces, ρ the materials density, $\boldsymbol{S}$ the first Piola-Kirchhoff stress tensor, $\boldsymbol{F}$ the deformation gradient tensor defined by:

$$\boldsymbol{F} = \mathrm{I} + \nabla \boldsymbol{u}, \tag{9}$$

where $\boldsymbol{I}$ is the identity tensor. The nonlinear deformation tensor is then given by:

$$\boldsymbol{\varepsilon} = \frac{1}{2}(\nabla \boldsymbol{u} + \nabla \boldsymbol{u}^{\mathrm{T}} + \nabla \boldsymbol{u} \cdot \nabla \boldsymbol{u}^{\mathrm{T}}). \tag{10}$$

The coupling with heat transfer is done through an additional deformation,

$$\boldsymbol{\varepsilon}_{th} = \alpha(T - T_{ref})\boldsymbol{I}, \tag{11}$$

where α is the thermal expansion coefficient of the materials and T_{ref} the reference temperature where there is no thermal expansion. The reference temperature for the Tokat is the solidus temperature whereas for the crucible steel it is 20 °C. An elastoplastic material model was used to describe the behavior of the Tokat. The crucible steel was described by a standard linear elastic model. Both were used allowing large deformations.

Modelling with Comsol Multiphysics

The full geometry is composed of the system to be cooled, of the surrounding air domain and of the infinite elements layer (Fig. 7). The edges of the cooling rings and the edges of the cooling tube belong to the boundaries of the simulation domain (Fig. 8). The modelling with Comsol Multiphysics is divided in six steps. The cooling rings have 24 holes equally spaced. The geometry of the part to be cooled was divided in 24 slices to make a as symmetric as possible mesh (Fig. 8).
Step 1: $t \in [0; 120]\ s$. The system to be cooled is removed from the furnace. Only the Heat Transfer in Solids and Fluids interface of the Heat Transfer Module is used to compute in the full domain the cooling by natural convection. The study is time

dependent. The equivalent heat transfer coefficient corresponding to the conductive heat flow through the boundaries of the cooled part is computed at each time step.

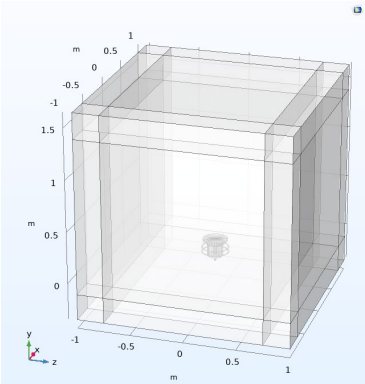

Figure 7. The full geometry representation in Comsol.

Step 2: The air flow field corresponding to the forced cooling is computed with the turbulent k-ε interface of the CFD Module in the surrounding air domain only. The computation uses the temperature distribution of the surrounding air reached at the end of Step 1. The study is time dependent. A ramping over ten seconds is made to increase smoothly the injection velocities. The velocity distribution solution is quasi-stationary. Thus, the computation was made over 30 seconds only (Fig. 9).

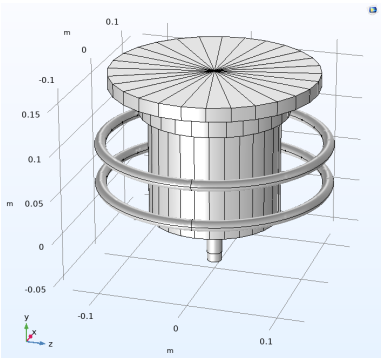

Figure 8. The cooling rings, the cooling tube and the system to be cooled represented in Comsol Multiphysics

Step 3: $t \in [120; 1200]\ s$. The Heat Transfer in Solids and Fluids interface of the Heat Transfer Module is used to compute in the full domain the cooling by forced convection. The stationary velocity field corresponding to the last step of Step 2 is used to define the convection in the surrounding air. The study is time dependent. The Nonisothermal Flow interface ensured the multiphysics coupling between the fluid flow and the heat transfer in the surrounding air. The Boussinesq approximation was selected for that coupling. A variable h_{eq} was created to compute the equivalent heat transfer coefficient corresponding to the conductive heat flow (Newton's law, [3]) through the boundaries of the cooled part at each time step:

$$h_{eq} = -\frac{ht.ndflux_u}{T - T_{amb}}\,. \tag{12}$$

Step 4: Step 1 and Step 3 were combined to get a continuous solution for the temperature and the equivalent heat transfer coefficient over the range $t \in [0; 1200]\ s$.
Step 5: $t \in [0; 1200]\ s$. The Heat Transfer in Solids and Fluids interface of the Heat Transfer Module was used to compute the cooling of the part by setting the equivalent heat transfer coefficient as the boundary condition in the Heat Flux field. The study was time dependent. The Niyama criterion was computed while solving ([5], [6],[7] and [8]). This required the implementation of a state variable.
Step 6: Step 5 allowed to detect the instant, t_S, from which the minimum solid fraction in the Tokat is 1. From that instant the Tokat is solid. Then, the Heat Transfer in Solids and the Solid Mechanics interfaces were coupled through Thermal Expansion in the Multiphysics node. The thermal expansion being applied only to the Tokat and to the steel crucible, a time dependent thermomechanical simulation was done in the range $t \in [t_S; 1200]\ s$. The elastoplastic material model describing the Tokat behaviour was based on the initial yield stress and the hardening function using equivalent plastic strains. A linear elastic model was used in the steel. The reference temperature for the thermal expansion in the Tokat was taken to be the solidus temperature whereas in the steel it was the standard reference temperature. The initial temperature distribution was the temperature field at the time t_S calculated in Step 5. The initial stress and deformation fields were calculated by a stationary computation using the initial temperature field. The activation node was used to prevent the Tokat from having initial elastic stress at the time t_S.

Simulation Results, Comparison with Experimental Measurements.

Figure 9 shows in representative cut plane the velocity field computed in Step 2.

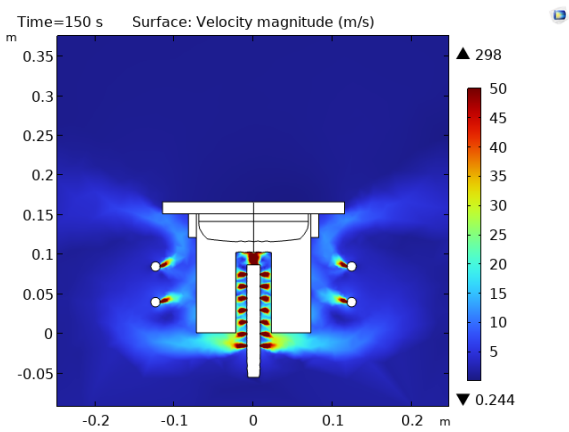

Figure 9. Velocity magnitude. The color range is enhanced to show the flow field.

Figure 10 shows the temperature distribution at the time 410 s during the forced cooling computed in Step 3.

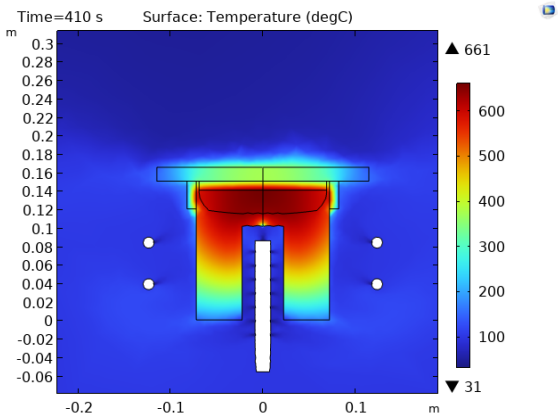

Figure 10. Temperature field at the beginning of the forced cooling.

Figure 11 is a zoom of Figure 10 showing the temperature distribution in the Tokat.

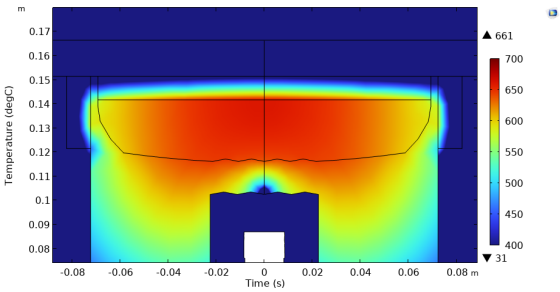

Figure 11. Temperature distribution in the Tokat in ºC at t = 410 s.

Figure 12 shows the comparisons of the temperature evolution between experiments and simulation at the location of the thermocouples. The qualitative evolution of the temperatures given by the simulation is coherent and fits well the experimental curves for T_1, T_2 and T_3 at the beginning of the cooling process. However, the cooling is too fast in the simulation in comparison with the curve representing T_4 and the temperatures at the centre and at the edge. The measurements were made in factory conditions which means less control on the measurement conditions even if they were made carefully. The simulation model didn't consider the base of the cooling station which probably has an influence on the air flow distribution on the bottom of the system and near the cooling tube. Figure 13 allows to understand the evolution of the solid fraction and the solidification front. It is expected to have a solidification front starting on the Tokat-steel interface from the bottom and going to the top. The heat transfer coefficient was found experimentally in the range 190-285 $W \cdot m^{-2} \cdot K^{-1}$ on the lateral boundary of the steel. The simulation gives the range 157-468 $W \cdot m^{-2} \cdot K^{-1}$.

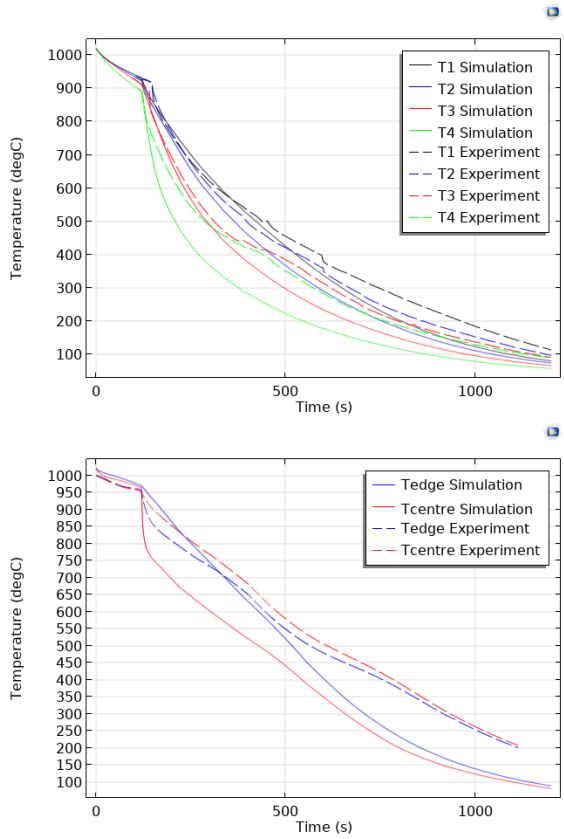

Figure 12. Comparison of the temperature evolution between simulation and measurements

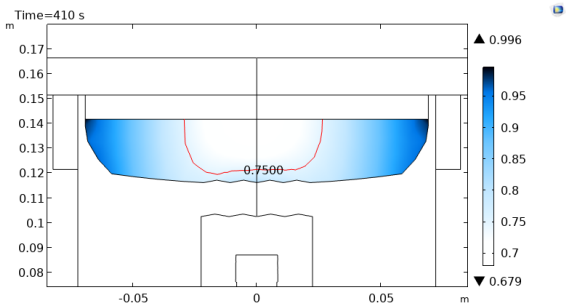

Figure 13. Solid fraction distribution in the Tokat showing the solidification front.

Figures 14-15 show the Niyama criterion and the residual von Mises Stress in the Tokat at the end of cooling. Figure 16 shows the evolution of the maximum von Mises stress.

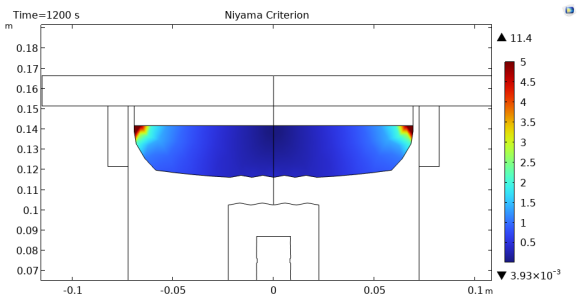

Figure 14. The Niyama Criterion in the Tokat.

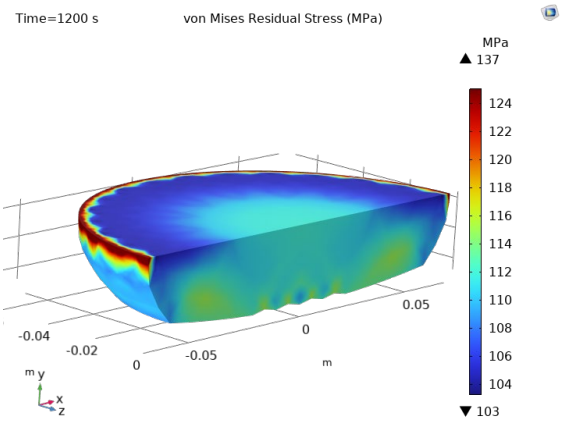

Figure 15. Von Mises residual stress in the Tokat.

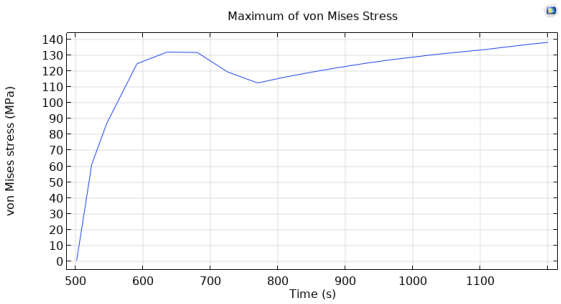

Figure 16. Evolution of the maximum von Mises stress in the Tokat.

We may notice the Niyama criterion is higher near the upper contact between the Tokat and the steel. At this location, the probability to have porosity is greater. The residual stresses are also higher at that location. The maximum Yield Strength of the Tokat is 110 MPa and the Ultimate Tensile Strength is 220 MPa, both at 20 °C. Thus, we have residual plastic deformations.

Conclusions

Comsol Multiphysics allowed to model the Kugler Bimetal process of cooling of bimetallic alloys. It was possible to couple three physics where we included user definitions of materials coming from laboratory characterization. The model we made gives coherent results in comparison with experiments. However, experiments were made in situ in the factory under real production conditions. This makes the comparisons more difficult because the factory environment cannot be fully controlled. The boundary conditions may be affected. We didn't model the base of the cooling system which has a posteriori an influence on the air flow distribution around the part. It was also not possible to guarantee the perfect contact and the position of the thermocouples in the steel inside the drilled holes. Measurements from several experiments show that this plays a significant role on the thermocouples' output. This was not represented in the numerical model, where the probes are directly located within the material bulk. The oxidation of the steel boundaries was not homogeneous. Further investigations must be done to check the impact on the heat transfer through these boundaries. An improved model of that complex process will have to integrate this tuning.

References

[1] A. Clarissou, V. Bruyere, P.Namy. I Crassous, Modeling of Thermal Expansion and Metallurgical Phases of a Material During Its Cooling, Proceedings of the Comsol International Conference, Münich 2023.
[2] Xiaoling Qi, Yahui Han, Yingda Wang, Hongbin Cai, Guoxiang Li, Effect of Casting Temperature on the Microstructure and Mechanical Properties of Cu-10Pb-10Sn/42CrMoS4 Bimetallic Hydraulic Cylinder Block, Journal of Materials Engineering and Performance (2024), https://doi.org/10.1007/s11665-023-09113-8.
[3] Jack. P. Holman, (2009), Heat Transfer., 10th Edition, McGraw-Hill, New-York.
[4] O. Pironneau, B. Mohammadi, Analysis of the k-epsilon Turbulence Model, 1994, Masson.
[5] Maodong Kang, Haiyan Gao, Jun Wang, Lishibao Ling, Baode Sun, Prediction of Microporosity in Complex Thin-Wall Castings with the Dimensionless Niyama Criterion, Materials 2013, 6, 1789-1802.
[6] Z. Ignaszak, Discussion on Usability of the Niyama Criterion for Porosity Predicting in Cast Iron Castings, Archives of Foundary Engineering, Vol. 17, Issue 3/2017, 196-204.
[7] Rouhollah Tavakoli, On the Prediction of Shrinkage Defects by Thermal Criterion Functions, Int. J. Adv. Manuf. Technol. 74, 569-579 (2014).
[8] Kent D. Carlson, C. Beckermann, Prediction of Shrinkage Pore Volume Fraction Using a Dimensionless Niyama Criterion, Metallurgical and Materials Transactions A, Vol. 40A, January 2009, 163-175.

Acknowledgements

The authors wish to kindly thank Innosuisse - Swiss Innovation Agency (Bern, Switzerland) for having supported this project (ref. 102.365).